



HAL
open science

Geometric evaluation of distortion correction methods in diffusion MRI of the spinal cord

Haykel Snoussi, Emmanuel Caruyer, Julien Cohen-Adad, Olivier Commowick,
Benoit Combes, Elise Bannier, Anne Kerbrat, Christian Barillot

► **To cite this version:**

Haykel Snoussi, Emmanuel Caruyer, Julien Cohen-Adad, Olivier Commowick, Benoit Combes, et al..
Geometric evaluation of distortion correction methods in diffusion MRI of the spinal cord. ISBI 2019
- 16th IEEE International Symposium on Biomedical Imaging, Apr 2019, Venice, Italy. pp.1696-1699,
10.1109/ISBI.2019.8759196 . inserm-01986723

HAL Id: inserm-01986723

<https://inserm.hal.science/inserm-01986723v1>

Submitted on 19 Jan 2019

HAL is a multi-disciplinary open access archive for the deposit and dissemination of scientific research documents, whether they are published or not. The documents may come from teaching and research institutions in France or abroad, or from public or private research centers.

L'archive ouverte pluridisciplinaire **HAL**, est destinée au dépôt et à la diffusion de documents scientifiques de niveau recherche, publiés ou non, émanant des établissements d'enseignement et de recherche français ou étrangers, des laboratoires publics ou privés.

GEOMETRIC EVALUATION OF DISTORTION CORRECTION METHODS IN DIFFUSION MRI OF THE SPINAL CORD

Haykel Snoussi¹ Emmanuel Caruyer¹ Julien Cohen-Adad² Olivier Commowick¹
Benoit Combes¹ Elise Bannier^{1,3} Anne Kerbrat^{1,3} Christian Barillot¹

¹ Univ Rennes, Inria, CNRS, Inserm, IRISA UMR 6074, Empenn ERL U 1228, Rennes, France

² NeuroPoly Lab, Institute of Biomedical Engineering, Polytechnique Montreal, Montreal, QC, Canada

³ CHU Rennes, Rennes, France

ABSTRACT

Acquiring and processing Diffusion MRI in spinal cord present inherent challenges. Differences in magnetic susceptibility between soft tissues, air and bone make the magnetic field of spinal cord non-uniform and inhomogeneous. In this context various procedures were proposed for correcting this distortion. In this work, we propose novel geometric statistics to measure the alignment of the reconstructed diffusion model with the apparent centerline of the spine. In parallel of the correlation with an anatomical T2-weighted image, we show the utility of these statistics to study and evaluate the impact of distortion correction by comparing 3 distortion correction methods from reversed gradient polarity strategy.

Index Terms— Diffusion MRI, Spinal Cord, Distortion correction

1. INTRODUCTION

Diffusion MRI (dMRI) is a unique MRI modality to map the in vivo geometry of neural architecture. Echo-planar images are sensitive to B0-field inhomogeneity; the resulting artefacts can severely affect image quality particularly in the spine region. However, strategies exist to correct these distortions, including co-registration, point spread function, phase field map and reversed gradient polarity method (RGPM). This pre-processing step is key to a number of analyses, including tractography and statistical analysis of scalar maps derived from the diffusion tensor such as fractional anisotropy (FA), axial diffusivity (AD) and radial diffusivity (RD).

In this work, we focus on the comparative evaluation of field inhomogeneity-induced distortion correction methods using RGPM, since the latter was shown to provide best results [1]. We propose a novel geometric method to measure the alignment of the reconstructed diffusion model with the apparent centerline of the spine. We use this measure and the correlation with an anatomical T2-weighted image to compare 3 distortion correction methods: HySCO [2] as implemented in ACID/SPM Toolbok, Topup [3] as implemented in FSL and Voss [4] (in-house implementation).

2. MATERIALS AND METHODS

2.1. Geometric measure of alignment

The diffusion tensor model relates the local displacement of water molecules with the surrounding tissue microstructure. In the spinal cord white matter, it is mainly aligned with longitudinal fibers [5], which themselves follow a path parallel to the centerline of the spinal cord. We can therefore expect that the principal eigenvector of the diffusion tensor is locally aligned tangentially with the centerline of the spine. However, when the image is distorted, the apparent shape of the spine is affected, while the direction of the tensor is not. This results in a poorer alignment of the diffusion tensor with the spine, locally. In what follows, we describe a method to measure how the diffusion tensors and the centerline align with each other.

Using a binary mask of the spine, we compute the centerline in two steps: first, for every axial slice, we compute the barycenter of the mask within this slice; then we fit a degree-3 smoothing spline to the set of barycenters. This provides us with a continuous, differentiable representation of the centerline, from which we can compute the Frenet frame. For a parametric curve $\mathbf{x}(t) \in \mathbb{R}^3$, the Frenet frame is defined as $(\mathbf{T}, \mathbf{N}, \mathbf{B})$ where \mathbf{T} is the tangent, \mathbf{N} is the normal and \mathbf{B} is the binormal (see Fig. 1):

$$\text{Tangent} \quad \mathbf{T} = \frac{d\mathbf{x}}{ds} = \frac{\mathbf{x}'}{|\mathbf{x}'|} = \frac{\mathbf{v}}{|\mathbf{v}|}$$

$$\text{Normal} \quad \mathbf{N} = \frac{d\mathbf{T}/ds}{|d\mathbf{T}/ds|} = \frac{\mathbf{T}'}{|\mathbf{T}'|}$$

$$\text{Binormal} \quad \mathbf{B} = \mathbf{T} \times \mathbf{N}$$

In the above, we use the curvilinear abscissa s , defined as

$$s(t) = \int_0^t |\mathbf{x}'(\tau)| d\tau,$$

and $\mathbf{v} = \mathbf{x}'$ is the velocity.

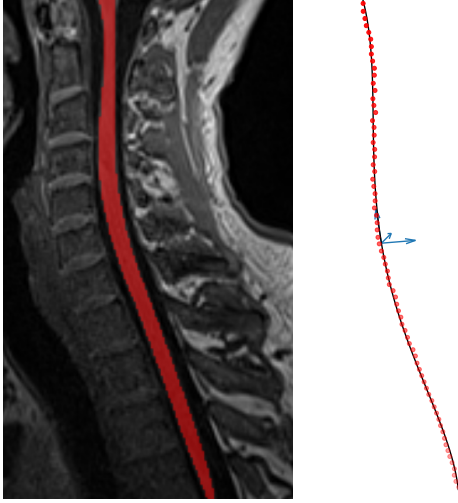


Fig. 1. (left) T1 image with segmented spinal cord for reference; (right) barycenters of the spline mask (red dots), fitted centerline (black line) and the Frenet frame (blue arrows).

For every voxel at position \mathbf{r} within the spinal cord, we compute the coordinates of the diffusion tensor principal eigenvector, $\mathbf{e}_1(\mathbf{r})$, in the Frenet frame computed at the closest point $\mathbf{x}(t_0)$ in the centerline: $t_0 = \arg \min_t \{|\mathbf{x}(t) - \mathbf{r}|\}$.

In order to summarize the distribution of $\mathbf{e}_1(\mathbf{r})$ over a region Ω , we compute the covariance matrix of these directions

$$\mathbf{M} = \frac{1}{\mathcal{V}(\Omega)} \int_{\Omega} \mathbf{e}_1(\mathbf{r}) \mathbf{e}_1(\mathbf{r})^T d\mathbf{r}.$$

where $\mathcal{V}(\Omega)$ is the volume of Ω . From the eigendecomposition of \mathbf{M} we extract two statistics: first the mean angle direction (MAD), defined as the angle between the principal eigenvector of \mathbf{M} and \mathbf{T} ; second the angular concentration of directions (ACD), defined as the first eigenvalue of \mathbf{M} . These stats were computed for $\Omega \in \{C1, \dots, C7, T1, T2, C1-C7, T1-T2\}$ corresponding to every cervical and thoracic vertebral levels.

2.2. Data acquisition

2.2.1. Patients and healthy volunteers

29 controls and 66 multiple sclerosis (MS) patients were recruited in the study from Rennes, Strasbourg, Marseille and Montpellier, approved by the local research ethics committee. All participants provided informed written consent.

2.2.2. MRI Acquisition

Images were acquired on a 3T Siemens Verio and a 3T Skyra scanners. Thirty non-collinear diffusion-weighted images (DWI) were acquired at $b = 900 \text{ s}\cdot\text{mm}^{-2}$, six non-DWI ($b =$

0) measurements and one non-DWI ($b = 0$) with an opposite phase encoding direction (PED) were also acquired. Scans were performed in sagittal orientation and head-foot (H-F) PED. The pulse sequence used for diffusion MRI is echo planar imaging (EPI). The reduced-FOV (field-of-view) technique was employed to reduce sensitivity of EPI to susceptibility artifacts. Sixteen slices were acquired with the following parameters without inter-slice gap: TR/TE = 3600/90 ms, with $2 \times 2 \times 2 \text{ mm}^3$ as the resolution, and image matrix 80×80 . The total acquisition time for the dMRI sequence was approximately 7 minutes. The protocol also includes two high-resolution anatomical references, T1-weighted image with an isotropic $1 \times 1 \times 1 \text{ mm}^3$ resolution and T2-weighted image with anisotropic $0.7 \times 0.7 \times 2.75 \text{ mm}^3$ resolution.

2.3. Pre-processing and metrics extraction

2.3.1. Diffusion MRI pre-processing

Motion between DWI were corrected using the Spinal Cord Toolbox (SCT) [6, 7]. Then, dMRI data were corrected for susceptibility distortion using the following three methods: Voss method [4] (in-house implementation), Topup implemented in FSL toolbox [3] and HySCO (Hyperelastic Susceptibility Artefact Correction) method [2] as implemented in ACID-SPM toolbox. In order not to bias the distortion correction comparison, we did a quality check to be sure that there no artifacts related to motion and ghosting in chosen data.

2.3.2. Segmentation

Using the Spinal Cord Toolbox (SCT) [7], whole spinal cord segmentation was carried out on T1-weighted, on T2-weighted and on the mean of corrected DWI volume ($b = 900 \text{ s}\cdot\text{mm}^{-2}$) by each method. A quality check was performed and manual adjustments were made when necessary.

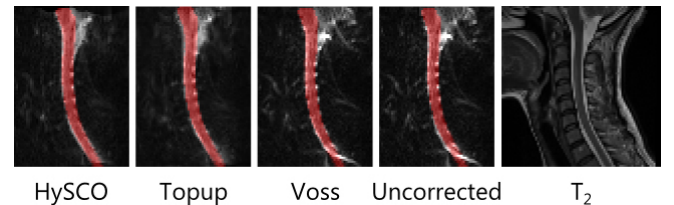


Fig. 2. Example of a corrected $b=0$ volume by each method and T2-weighted rigidly registered.

2.3.3. Template-based analysis

Next, DWI data were registered to the PAM50 spinal cord template [8], using a various affine and homeomorphic transformation between the mean of the DWI, PAM50 template

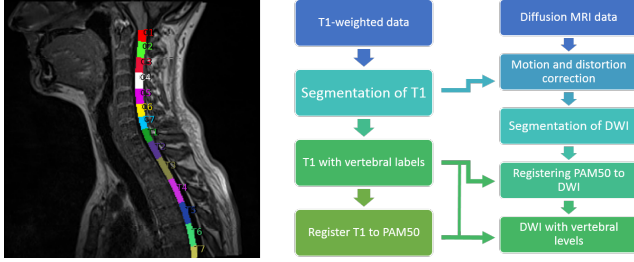


Fig. 3. Left: T1 image with vertebral labels; right: imaging and processing pipeline for diffusion MRI and T1 images.

[7] and the T1-weighted anatomical data as it has isotropic resolution. Alignment with the template provides robust definition of the inter-vertebral levels for the spine. This enables computation of the average metrics in spinal cord using the atlas-based approach introduced in [9], which overcome biases related to partial volume effects. As a result, we can quantify diffusion-based metrics averaged for each inter-vertebral level between C1 and T2. The processing pipeline is summarized in Fig. 3.

3. RESULTS

3.1. Geometric statistics

For every distortion correction method, geometric stats were computed for every cervical and thoracic levels; paired t-test was computed to compare the performance of each method to the non-corrected dMRI. Results of p-values and t-statistic are presented in tables 2 and 1. Green and red indicate significant improvement and significant deterioration, respectively.

3.2. Cross-correlation study

Cross-correlation was computed between first $b=0$ volume of uncorrected and each corrected dMRI, and the rigidly registered T2-weighted only within the overlap between mask of DWI and the rigidly registered mask of T2-weighted (Fig. 2). We calculate cross-correlation for the whole spinal cord. A Tukey test was performed on the cross-correlation scores and reported in Table. 3. Note that results presented here are slightly different to the study reported in [1] because of some difference in pipeline treatment. In (Fig. 4) results in boxplot format.

4. DISCUSSION

For HySCO, as shown in Table. 1, for MAD metric we can observe that it performs significantly better than uncorrected in T1 and T2 vertebral levels. For ACD metric we remark a significant improvement at edges of the spinal cord (C1 and

| | HySCO | | Topup | | Voss | |
|------|---------|------|---------|------|---------|------|
| | P-value | t | P-value | t | P-value | t |
| C1 | 0.46 | -0.7 | 0.40 | -0.8 | 0.04 | -2.0 |
| C2 | 0.01 | 2.4 | 0.01 | 2.4 | 0.17 | 1.3 |
| C3 | 0.15 | -1.4 | 0.91 | 0.1 | 0.13 | -1.4 |
| C4 | 0.91 | -0.1 | 0.08 | 1.7 | 0.62 | -0.4 |
| C5 | 0.26 | 1.1 | 0.004 | 2.8 | 0.30 | 1.0 |
| C6 | 0.71 | -0.3 | 0.11 | 1.5 | 0.74 | -0.3 |
| C7 | 0.94 | -0.1 | 0.62 | 0.4 | 0.62 | -0.4 |
| T1 | 0.02 | -2.2 | 0.79 | 0.2 | 0.03 | 2.1 |
| T2 | 0.01 | -2.4 | 0.39 | 0.8 | 0.43 | 0.7 |
| C1-7 | 0.43 | -0.7 | 0.15 | 1.4 | 0.05 | -1.9 |
| T1-3 | 0.35 | -0.9 | 0.07 | 1.8 | 0.25 | 1.1 |

Table 1. Comparison of the Mean Angle Direction (MAD) between non-corrected images and HySCO, Topup and Voss: results of the paired t-test per vertebral level. If t-statistic value is negative, this means that the mean angle direction in the corrected images is better than in the uncorrected images.

T1), for whole of cervical and thoracic parts as shown in Table. 2. For Topup, there is some significant improvement for the angular concentration in some levels, not part. However, we remark significant deterioration in the mean angle direction in C2 and C5 levels. For Voss method, there a slight improvement in MAD metric but a very remarkable amelioration for angular concentration of directions in all levels and parts of the spinal cord, exception C3 and C4 which are in the middle of the field-of-view of the acquisition. For cross-correlation, there no significant amelioration as demonstrated in Table. 3.

5. CONCLUSION

We proposed geometrical metrics to measure the impact of distortion correction in diffusion MRI of the spinal cord. Based on the assumption that the distortion only affects the apparent shape of spine and not the principal direction of diffusion, we proposed two novel statistics which take into account the alignment of the diffusion tensor with the apparent centerline of the spinal cord. This geometric evaluation was used to compare 3 distortion correction methods conducted on 95 scans. The fragmentation by levels and parts of the spine shows the different impact between edges (C1, C2, T1, T2) and center (C3,C4) of the imaging window. This local evaluation provides a performance measure complementary to classical comparison with a reference anatomical image.

| | HySCO | | Topup | | Voss | |
|------|-------------|------|-------------|------|--------------|-----|
| | P-value | t | P-value | t | P-value | t |
| C1 | 0.05 | 1.8 | 0.31 | 1.0 | 7.10^{-3} | 2.7 |
| C2 | 0.97 | -0.1 | 0.02 | 2.2 | 0.01 | 2.5 |
| C3 | 0.40 | 0.8 | 0.61 | 0.5 | 0.21 | 1.2 |
| C4 | 0.69 | -0.3 | 0.21 | -1.2 | 0.37 | 0.8 |
| C5 | 0.41 | -0.8 | 0.03 | 2.1 | 0.03 | 2.1 |
| C6 | 0.13 | -1.5 | 0.01 | 2.4 | 7.10^{-5} | 4.1 |
| C7 | 0.05 | -1.9 | 0.34 | 0.9 | 7.10^{-3} | 2.7 |
| T1 | 0.03 | 2.1 | 0.21 | 1.2 | 0.04 | 1.9 |
| T2 | 0.10 | 1.6 | 7.10^{-4} | 3.5 | 7.10^{-5} | 4.2 |
| C1-7 | 3.10^{-5} | 4.3 | 0.24 | -1.1 | 7.10^{-12} | 7.8 |
| T1-3 | 0.01 | 2.5 | 0.65 | 0.4 | 10^{-12} | 8.1 |

Table 2. Comparison of the Angular Concentration of directions (ACD) between non-corrected images and HySCO, Topup and Voss: results of the paired t-test per vertebral level. If t-statistic value is positive, this means that the angular concentration in the corrected images is better than in the uncorrected images.

| Methods | HySCO | Topup | Voss |
|-------------|-------|-------|--------|
| P-value | 0.062 | 0.072 | 0.355 |
| t-statistic | 1.882 | 1.814 | -0.927 |

Table 3. Comparison of the cross-correlation between T2w and the corrected b=0 diffusion image between non-corrected image and HySCO, Topup and Voss: results of the paired t-test for the whole cervical spine.

6. ACKNOWLEDGMENT

Haykel Snoussi was partly funded by the EMISEP PHRC, the Brittany region and a MITACS-Inria Globalink travel grant. MRI data acquisition was supported by the Neurinfo MRI research facility from the University of Rennes 1. We thank Benjamin De Leener and Charley Gros from NeuroPoly Lab for their help.

7. REFERENCES

[1] H Snoussi, E Caruyer, O Commowick, E Bannier, and C Barillot, “Comparison of inhomogeneity distortion correction methods in diffusion mri of the spinal cord,” in *ESMRMB-34th Annual Scientific Meeting*, 2017.

[2] L Ruthotto, H Kugel, J Olesch, B Fischer, J Modersitzki, M Burger, and CH Wolters, “Diffeomorphic susceptibility artifact correction of diffusion-weighted magnetic resonance images,” *Physics in Medicine & Biology*, vol. 57, no. 18, pp. 5715, 2012.

[3] Jesper LR Andersson, Stefan Skare, and John Ashburner,

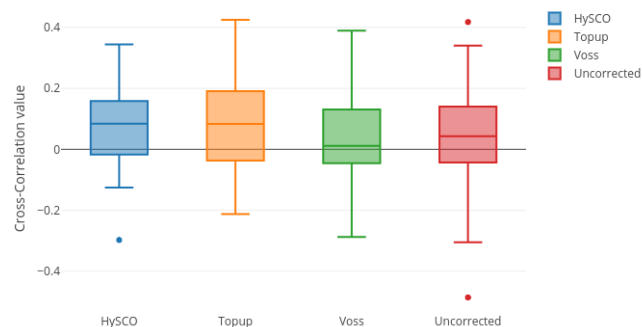


Fig. 4. Cross-correlation between T2w and the corrected b=0 diffusion image

“How to correct susceptibility distortions in spin-echo echo-planar images: application to diffusion tensor imaging,” *Neuroimage*, vol. 20, no. 2, pp. 870–888, 2003.

[4] H U Voss, R Watts, A M Uluğ, and D Ballon, “Fiber tracking in the cervical spine and inferior brain regions with reversed gradient diffusion tensor imaging,” *Magn reson imaging*, vol. 24, no. 3, pp. 231–239, 2006.

[5] J Cohen-Adad, M Descoteaux, S Rossignol, R D Hoge, R Deriche, and H Benali, “Detection of multiple pathways in the spinal cord using q-ball imaging,” *Neuroimage*, vol. 42, no. 2, pp. 739–749, 2008.

[6] J Xu, J S Shimony, E C Klawiter, A Z Snyder, K Trinkaus, R T Naismith, T LS Benzinger, A H Cross, and SK Song, “Improved in vivo diffusion tensor imaging of human cervical spinal cord,” *Neuroimage*, vol. 67, pp. 64–76, 2013.

[7] B De Leener, S Lévy, S M Dupont, V S Fonov, N Stikov, D L Collins, V Callot, and J Cohen-Adad, “SCT: an open-source software for processing spinal cord MRI data,” *Neuroimage*, vol. 145, pp. 24–43, 2017.

[8] Benjamin De Leener, Vladimir S Fonov, D Louis Collins, Virginie Callot, Nikola Stikov, and Julien Cohen-Adad, “Pam50: Unbiased multimodal template of the brainstem and spinal cord aligned with the icbm152 space,” *NeuroImage*, vol. 165, pp. 170–179, 2018.

[9] Simon Lévy, M Benhamou, C Naaman, Pierre Rainville, Virginie Callot, and Julien Cohen-Adad, “WM atlas of the human spinal cord with estimation of partial volume effect,” *Neuroimage*, vol. 119, pp. 262–271, 2015.